

Determine Perceptual Laser Modulation Threshold for Embedding Sinusoidal Signature in Electrophotographic Half-toned Images

Pei-Ju Chiang¹, Edward J. Delp², Jan P. Allebach², George T.-C. Chiu¹

¹School of Mechanical Engineering, ²School of Electrical and Computer Engineering
Purdue University,
West Lafayette, Indiana

Abstract—Printer identification based on a printed document can provide forensic information to protect copyright and verify authenticity. In addition to intrinsic features (intrinsic signatures) of the printer, modulating the printing process to embed specific signatures (extrinsic signatures) will further extend the encoding capacity and utility. One of the key issues with embedding extrinsic signature is the embedded signature should not be detectable by the human observer but is detectable using a matched sensing device and detection algorithm. In this paper, we will investigate the modeling and experimental characterization of the EP process to obtain the modulation threshold such that the embedding signatures are below human visual threshold. An empirical model is established and a heuristic functional inverse is used to obtain the process modulation threshold.

Index Terms—Extrinsic signature, laser intensity modulation, human visual system, modulation threshold.

I. INTRODUCTION

BANDING is one of the image artifacts for electrophotographic (EP) printers, e.g. laser printer. It manifests as contrast variations on a printed page and is especially visible in the mid-tone area. Many approaches have been shown to be effective in reducing banding by modulating EP process parameters such as laser intensity or timing [1-2] and motor speed [3] to compensate for process disturbances such as gear noise. These methods can also be used to inject properly designed banding signatures. Due to its origin within the EP process, banding can be viewed as an intrinsic signature [4-10] of the specific printer. Modulating the EP process to generate banding signals that are below human visual threshold but can be detected by effective detection approach can further extend the signature capacity and capability. The ability to precisely control the EP process and modulate unperceivable but detectable banding is essential.

In our previous work [11-16], we have reported techniques of

modulating the exposure of the EP process through laser intensity modulation and embedding information in documents. In this paper, we will discuss a combined physical and empirical model based approach to obtain modulating threshold for electrophotographic half-toned images. Experimental results using an off-the-shelf office laser printer will be presented to verify the effectiveness of the proposed technique.

The remaining of the paper is organized as follows. Laser intensity modulation is presented in the next section followed by model of human visual system. The discussion of laser modulation threshold will be presented in the forth section followed by experimental validation. Finally, the conclusions are given in the last section.

II. LASER INTENSITY MODULATION

Modulating the laser intensity effectively modulates the exposure process on the surface of the Organic photoconductor (OPC) drum and changes the size of the dots (dot gain) form by the toner particles. The changes in dot gain result in changes in effective contrast as viewed by the human observer. Introducing periodic modulation in the laser intensity will result in harmonic contrast modulation of the printed image that can be detected after the image is scanned. This is the fundamental process for embedding extrinsic signatures into a document. Figure 1 shows basic process block diagram of embedding banding signals by modulating the laser intensity in an EP process.

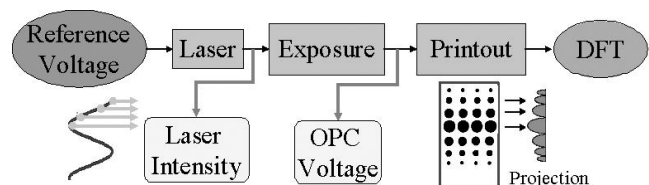


Figure 1 Process block diagram for embedding and detecting extrinsic banding signature using laser intensity modulation

To take advantage of the effect of laser intensity on the EP process, a combined physical and experimental EP process model with laser intensity as input and dot gain as output need to be developed. The intensity profile of the laser is modeled as a

2-D Gaussian envelope [17, 18] given by

$$I(x, y, t) = I_0(t) e^{-(y^2/2\alpha^2 - x^2/2\beta^2)} \quad [W/m^2], \quad (1)$$

where $I_0(t)$ represents the power amplitude of the laser, and β and α are the beam widths in the scan x , and process y , directions, respectively. Assume the laser is switched on at time 0 and off at time t_{off} . Since the beam will not reach its peak intensity I_{max} and reach zero when it is turned off instantaneously, the rise and fall transition are modeled as exponential functions, see Figure 2. The laser intensity profile can be expressed as

$$I_0(t) = \begin{cases} 0, & t < 0, \\ I_{max} (1 - e^{-\frac{t}{t_r}}), & 0 \leq t \leq t_{off}, \\ I_{max} (1 - e^{-\frac{t_{off}}{t_r}}) \cdot e^{-\frac{-(t-t_{off})}{t_f}}, & t > t_{off}, \end{cases} \quad (2)$$

where t_r is the rise time constant (sec), t_f is the fall time constant (sec).

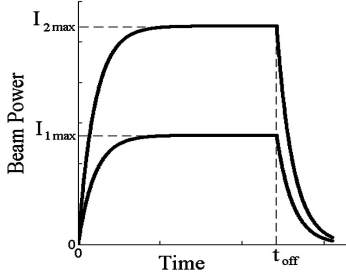


Figure 2 Temporal response of a laser pulse

As shown in Figure 2, when I_{max} increases, the maximum value of $I_0(t)$ increase as well. Since the laser intensity is taken to be proportional to the laser diode current, which is proportionally controlled by the reference voltage V_r on the laser driver chip, the peak intensity I_{max} can be expressed as:

$$I_{max}(t) = \lambda V_r \quad [W/m^2] \quad (3)$$

where λ is the ratio of V_r to intensity I_{max} . Let the nominal values of the printed pixel width in the scan direction and process direction be X and Y , respectively. Assume the laser beam translates along the scan direction x at a velocity v (m/sec), which is significantly higher than the liner motion of the photoconductor surface in the process direction. The exposure energy at any arbitrary point (x, y) on the OPC due to the pixel $[m, n]$ being turned on is found by integrating Eq. (1) with respect to time, i.e.

$$E_{mn}(x, y) = \int I_0(t) \exp\left(-\frac{(y - y_n)^2}{2\alpha^2} - \frac{(x - (x_m - X/2) - vt)^2}{2\beta^2}\right) dt \quad [J/m^2] \quad (4)$$

Since the exposure energy at an location on the OPC due to each printed pixel is additive, the overall exposure at any given point on the OPC surface is the sum of exposures contributed from each neighboring pixel in the halftone, i.e.

$$E(x, y) = \sum_{m,n} E_{mn}(x, y) \quad (5)$$

After the photoconductor is exposed by the laser, the associated exposure $E(x, y)$ forms a latent image on the photoconductor surface. Charged toner particles are attracted to the latent image through an electrostatic field and subsequently transferred and fused to paper. Based on the discharged electric potential characteristic of the photoconductor material, the tone value adhered on the photoconductor can be estimated. Here, the photoconductor surface voltage after exposure, i.e. the light voltage V_L [17] can be written as

$$V_L = V_{sat} + (V_D - V_{sat}) \exp\left(\frac{-E}{E_a}\right) \quad \text{Volts} \quad (6)$$

where V_{sat} is the saturation voltage due to high exposure energy, V_D is the dark voltage, E is the exposure energy, and E_a is a coefficient that characterize the exposure sensitivity of the photoconductor. Through modulating the reference voltage V_r , the exposure energy and the associated photoconductor surface voltage are adjusted. This will affect the probability and the number of toner particles being transferred (developed) on to the OPC surface and results in subsequent modulation of the density of the toner particles developed (developed solid area density) and the size of the developed toner dots (dot size/dot gain). The relationship between developed solid area density and photoconductor surface voltage is nonlinear and can be found in [19].

Figure 3 shows the relationship between the laser intensity reference voltages and the measured dot size on paper. The dot size is determined by counting the number of pixels with an absorbance greater that 0.1 in one dot cell. As seen in Figure 3, measured dot size increases with increase of the reference voltage. As expected, the uncertainty and fluctuation in the EP process results in fluctuation in the corresponding dot sizes. Through periodic dot sizes modulation, extrinsic banding (signatures) can be embedded.

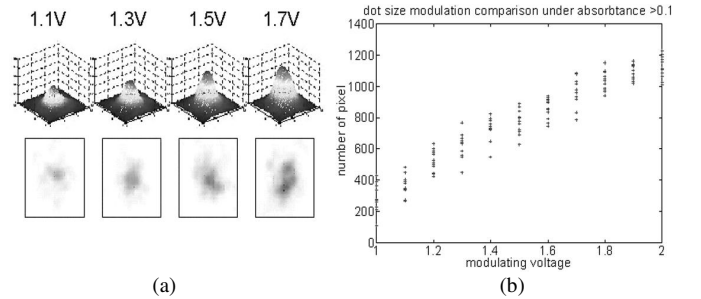


Figure 3 Relationship between laser intensity and dot size

III. MODEL OF HUMAN VISUAL SYSTEM

In order to embed unperceivable extrinsic signature, a model of the human visual system (HVS) is needed. One of such model is the contrast sensitivity function (CSF) that attempts to capture the modulation transfer function (MTF) of the human visual system in perceiving contrast variations. In this work, we report one of the most widely used CSF model [20] by fitting

psychophysical experiment data with the following exponential function

$$S_c(f, Y_0, W, \theta) = a(f, Y_0, W) f e^{-\Gamma(\theta) b(Y_0) f} \sqrt{1 + c e^{b(Y_0) f}} \quad (7)$$

where

$$a(f, Y_0, W) = \frac{540(1 + \frac{0.7}{Y_0})^{-0.2}}{1 + \frac{12}{W(1 + \frac{f}{3})^2}}$$

$$b(Y_0) = 0.3(1 + \frac{100}{Y_0})^{0.15}$$

$$c = 0.06$$

$$\Gamma(\theta) = 1.08 - 0.08 \cos 4\theta$$

In the above equations, the angular frequency of the stimulus f is measured in cycles/degree; W is the angular display size in degrees calculated from the square root of the picture area; Y_0 is the mean local background luminance in cd/m^2 , and θ the orientation of the stimulus in radius.

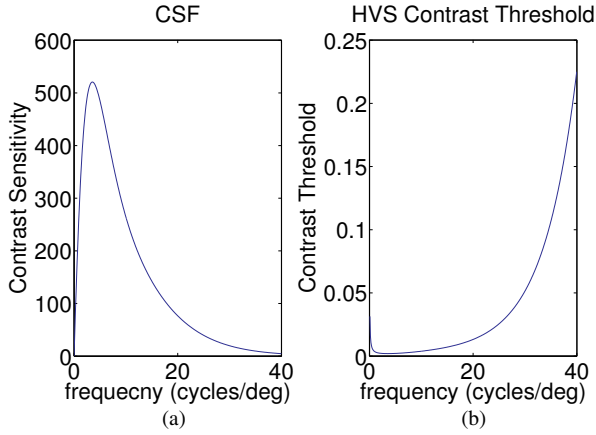


Figure 4. (a) Human contrast sensitivity function (CSF); (b) the corresponding human visual system (HVS) contrast threshold

In Figure 4(a) the plots of the CSF with respect to the angular frequency are reported for a background luminance of $50 cd/m^2$ with a horizontal stimulus ($\theta = 0$) and $180/(\pi\sqrt{12})^5$ degree angular display size using a test pattern with height h and width $4h/3$ is viewed from a distance of four times its height. As shown in Figure 4(a), the CSF functions as a band-pass filter reflecting the band-pass nature of the human visual system that is less sensitive to low and high frequency contrast variation (bandings). The low and high frequency regions can be exploited to embed unperceivable signatures. Figure 4(b) illustrates the contrast threshold of HVS where the y-axis indicates the reciprocal of contrast sensitivity. The threshold information is important since the signature should be below the perception threshold. The modulating parameter, the laser intensity in this case, and the resulting contrast variation need to be below the human detection threshold.

Since the printer is a nonlinear system, with sinusoidal process parameter modulation, in this case, the laser intensity, the resulting variation in luminance of the printout will not be

sinusoidal. A convenient technique for calculating the luminance distribution of a non-sinusoidal grating is to consider separately the imaging of each of the Fourier components of the grating wave form. According to Campbell's experiments [21], grating of complex wave form cannot be distinguished from sine wave grating until their contrast has been raised to a level at which the higher harmonic components reach their independent threshold. If the amplitude of Fourier components of high harmonic frequencies is lower than the fundamental, the contrast threshold of a grating is determined only by the amplitude of the fundamental Fourier component of its wave form. We will be using Campbell's finding to obtain laser intensity modulation threshold based on a gray-box model of the EP process.

IV. LASER MODULATION THRESHOLD

As discussed in the previous section, to embed unperceivable banding signal in EP printed document, the resulting contrast variation due to the embedded signal needs to be below the human contrast sensitivity threshold. Since the laser intensity is the actual input signal, it is therefore important to derive the corresponding laser intensity modulation threshold.

The laser intensity modulation is done by modulating the voltage of the laser intensity control signal V_r

$$V_r = V_0 + V_{mod}, \quad (8)$$

where V_0 denote the nominal voltage to the laser power control circuit during normal operation and V_{mod} denote the modulation. To maintain process stability, V_r is constricted between a pair of minimum value V_{min} and maximum value V_{max} .

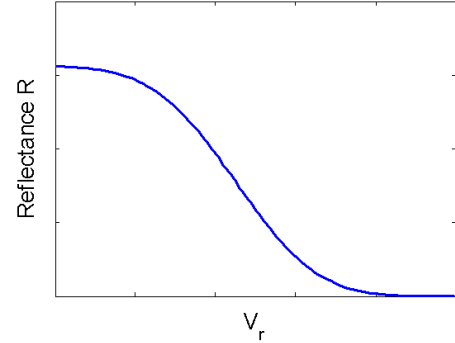


Figure 5. Relationship between laser intensity and reflectance R

Since higher laser intensity will result in higher exposure energy, more toner will be attracted to the OPC that will result in lower reflectance. Figure 5 shows the average reflectance measured from a test patch with different laser intensity, i.e. different V_r values. Note that at low intensity, very little toner is developed and no reflectance change is observed. At high intensity, the number of toner particles increase to a value that majority of the lights are trapped and the reflectance 'saturate' to a minimum value. To fit the experimental data shown in Figure 5, we will use a third order polynomials function,

$$R(V_r) = \sum_{i=0}^3 a_i \left(\frac{V_r - V_0}{V_b} \right)^i, \quad (9)$$

where $V_b = \min\{|V_0 - V_{max}|, |V_0 - V_{min}|\}$ is the maximum applicable modulation amplitude, and a_i are the corresponding coefficients.

In the current implementation, the laser intensity modulation is done on a scan-line by scan-line basis, i.e. the laser intensity is the same for each scan-line (x direction) and is change from scan-line to scan-line in the process (y) direction. For sinusoidal modulation, the modulation term in Eq. (8) can be written as

$$V_{\text{mod}}(y) = \Delta V \sin(w_m y) = V_b \cdot \alpha \sin(w_m y) \quad (10)$$

where ΔV is the modulation amplitude, $\alpha = \Delta V/V_b$ is the normalized modulation amplitude, w_m is the spatial modulation frequency in cycles per inch, and y is the coordinate in process direction in inch.

Since the mapping between V_r and reflectance R is nonlinear, introducing sinusoidal modulation in the laser intensity will result in contrast variation with harmonics in addition to the fundamental frequency, i.e.

$$R(y) = \sum_{i=0}^3 a_i [\alpha \sin(w_m y)]^i = \sum_{i=0}^3 k_i \sin(iw_m y) \quad (11)$$

where $k_0(\alpha) = a_0 + \frac{1}{2}a_2\alpha^2$, $k_1(\alpha) = a_1\alpha + \frac{3}{4}a_3\alpha^3$, $k_2(\alpha) = -\frac{1}{2}a_2\alpha^2$ and $k_3(\alpha) = -\frac{1}{4}a_3\alpha^3$.

To generate a desired tone value, an associated halftone pattern is tiled across the whole image. Since the halftone pattern is repeated in both of scan (x) and process (y) directions, the image projection in the process direction is a periodic signal with the halftone frequency w_h depending on the size of the halftone pattern. Since any periodic signal can be presented with it unique Fourier series, the projected luminance value can be decomposed into several sinusoidal components with frequency iw_h and amplitude b_j , where j is an integer between 0 and the order of Fourier series expansion n . Since the luminance is proportional to reflectance, sinusoidal modulation in laser intensity will results in luminance variation in the form

$$Y(y) = \left[\sum_{i=0}^3 k_i \sin(iw_m y) \right] \left[\sum_{j=0}^n b_j \sin(jw_h y) \right] \quad (12)$$

$$= \sum_{i=0}^3 \sum_{j=0}^n \frac{k_i b_j}{2} [-\cos(iw_m y + jw_h y) + \cos(iw_m y - jw_h y)]$$

As shown in Eq. (5), the overall exposure at any given point on the OPC surface is the sum of exposures contributed from each neighboring pixel. Adjacent horizontal scan-lines overlap one another by an amount that depends on the relative spot size and scan-line separation. This will constrict the printer resolution to address the fine details that is often characterized by the printer's modulation transfer function (MTF). As the embedding laser modulation frequencies increases, smaller dots

will be more difficult to preserve because of overlapping of surrounding larger dots. This results in the degradation of the contrast that can also be characterized by a low pass filter (LPF). For modeling the effect of embedding sinusoidal extrinsic signature using laser intensity modulation, the printer model can be characterized as a sequential combination of a nonlinear mapping between intensity V_r and reflectance R , a combined halftone and low-pass filter from reflectance to measured luminance Y as depicted in Figure 6. Let the magnitude of the low pass filter at frequency w be $q(w)$. The resulting contrast C at each frequency component w_{ij} will be:

$$C_{i,j} = \frac{\Delta Y_{i,j}}{Y_0} = \frac{|k_i(\alpha) b_j / 2| \cdot q(w_{i,j})}{Y_0} \quad (13)$$

where $w_{i,j} = iw_m \pm jw_h$ and $\Delta Y_{i,j}$ is the resulting luminance value at frequency $w_{i,j}$.

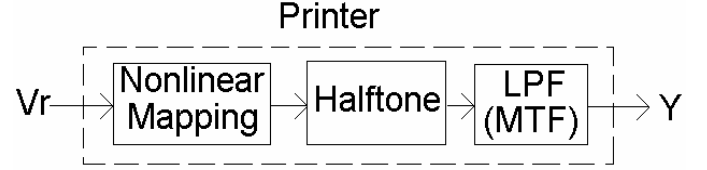


Figure 6. Block diagram of printer model for modeling embedding sinusoidal signal using laser intensity modulation

To embed unperceivable banding signal in a printer document, the resulting contrast at each frequency component needs to be below the human contrast sensitivity threshold C_{TH} , i.e., $C_{i,j} \leq C_{TH}$. The corresponding laser intensity modulation threshold can be calculated as:

$$\alpha = \min_{i,j} \Delta Y_{i,j}^{-1} (C_{TH}(w_{i,j}) Y_0) \quad (14)$$

V. EXPERIMENTAL RESULTS

In this work, we used a calibrated EPSON 3200 flatbed scanner to measure the corresponding CIE Y luminance (defined by International Commission on Illumination) of the test pages. The calibration curve of the scanner from 8 bit values to luminance is shown in Figure 7. Because of different printing techniques, every printer generates different luminance value given the same 8 bit uniform gray image. Therefore, the parinter of interest will also need to be calibrated. In practice, the specific printer calibration can be obtained by the tone correction curve unique to each printer and stored either in the nonvolatile memory of the printer or the host computer. In the case when calibration curve is not available, but the printed is accessible, calibration procedure can be performed. Test pages with 10 Post Script (PS) gray fill using the printer's default halftone are printed with nominal laser intensity V_r . The measured mean luminance corresponding to various gray fill is shown in Figure 8. Since human visual system (HVS) is more sensitivity to mid-tone images, in the following work, images with background luminance 50 cdl/m^2 , i.e. PS gray fill 0.8., is used to measure the modulation threshold. The reflectance

corresponding to different laser intensity V_r for PS gray fill 0.8 is measured and shown in Figure 9. The data in Figure 9 is used to calculate the polynomial coefficient of Eq. (9).

To characterize the gain of the effective LPF on luminance, various normalized modulation amplitude α ranged from 0.1 to 0.7 with 0.2 increments are applied. For each α value, a modulation frequency from 50 cycles/in (10.5 cycles/deg) to 170 cycles/in (35.6 cycles/deg with 12 inch view distance) at 20 cycles/in increment is applied. The luminance magnitude at each modulation frequencies for various modulation amplitudes are measured and shown in Figure 10(a). An exponential function

$$q(w) = e^{-\beta w} \quad (16)$$

can be fitted to the normalized magnitude value at spatial frequency w in cycles/deg with decay rate β , see Figure 10(b). The luminance value at frequency $w_{i,j}$ is:

$$\Delta Y_{i,j} = \left| \frac{k_i b_j}{2} \right| e^{-\beta w_{i,j}} \quad (17)$$

where the mean value of β is 0.0779. Laser intensity modulation threshold can then be obtain by numerically solving Eq. (14), as shown in Figure 11. Periodic banding signature generated from modulation amplitude α under the threshold will not be perceivable. From Figure 11, higher modulation threshold in high frequencies indicates that high spatial frequency provide the better trade-off between perceptibility and signal intensity that is directly related to detectability and capacity.

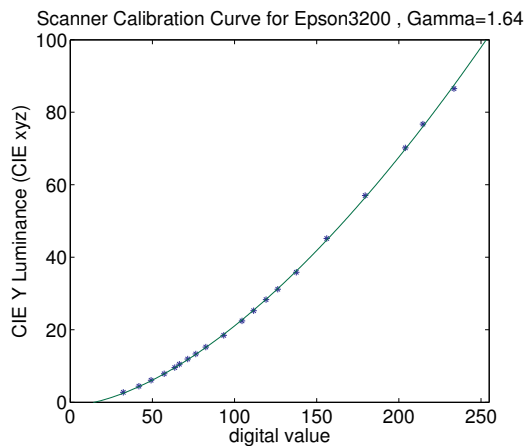


Figure 7. Scanner calibration curve for Epson 3200

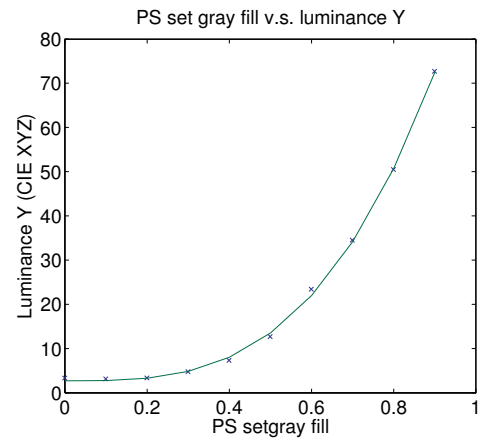


Figure 8. Printer tone curve

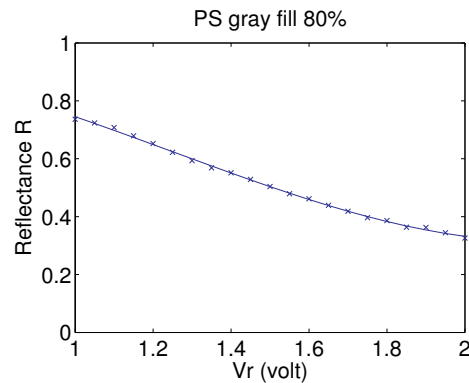


Figure 9. Relationship between laser intensity and luminance

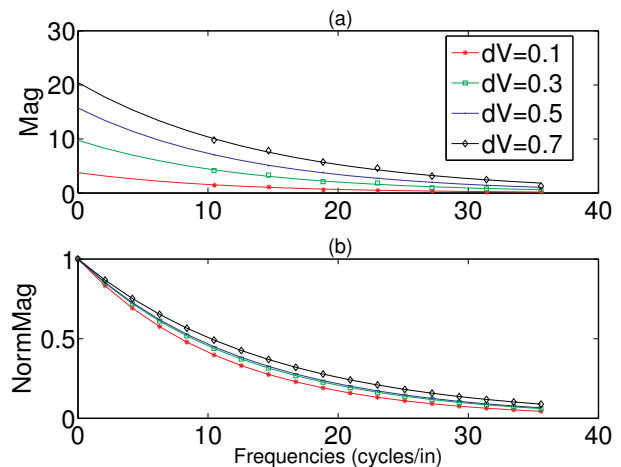


Figure 10. Measured and normalized luminance as a function of modulation frequency

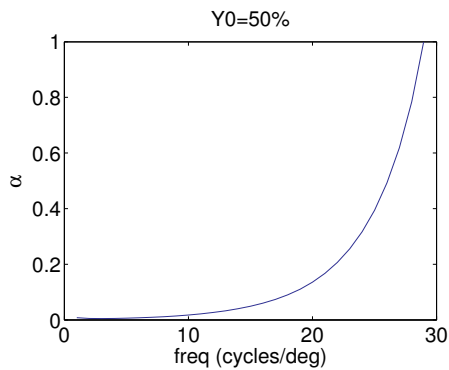


Figure 11. Laser intensity modulation threshold

VI. CONCLUSION

In this work, modeling and experimental characterization of an EP process to enable embedding banding signal that are below human visual threshold is presented. The results provide the necessary information for embedding extrinsic signature as well as provided design thresholds for printer developer to reduce the intrinsic banding signal in an EP process. As predicted that high spatial frequency provided the better trade-off between perceptibility and embedding capacity.

ACKNOWLEDGMENT

The author would like to acknowledge the support of the United States National Science Foundation under the grant CCR-0524540.

REFERENCES

- [1] G.Y. Lin, J. Grice, J. Allebach, G. T.-C. Chiu, W. Bradburn, and J. Weaver, "Banding Artifact Reduction in Electrophotographic Printers by Using Pulse Width Modulation", *Journal of Image Science and Technology*, Vol. 46, No. 4, pp.326-337, 2002.
- [2] D. Kacker, t. Camis and J. P. Allebach, electrophotographic Process Embedded in Direct Binary Search, *IEEE Trans. On Image Processing*, 11, p234-257, 2002.
- [3] C.-L. Chen, G. T.-C. Chiu, and J. P. Allebach, "Banding Reduction in Electrophotographic Processes Using Human Contrast Sensitivity Function Shaped Photoconductor Velocity Control", *Journal of Image Science and Technology*, Vol. 47, No. 3, pp. 209-223, 2003.
- [4] G. N. Ali, P.J. Chiang, A. K. Mikkilineni, J. P. Allebach, G. T. C. Chiu and E. J. Delp, "Intrinsic and Extrinsic Signatures for Information Hiding and Secure Printing with Electrophotographic Devices", in *Proceedings of the IS&T's NIP19: International Conference on Digital Printing Technologies*, New Orleans, 2003, pp. 511-515.
- [5] G. N. Ali, A. K. Mikkilineni, P. J. Chiang, J. P. Allebach, G. T. C. Chiu and E. J. Delp, "Application of Principal Components Analysis and Gaussian Mixture Models to Printer Identification", in *Proceedings of the IS&T's NIP20: International Conference on Digital Printing Technologies*, 2004, pp. 301-305.
- [6] A. K. Mikkilineni, P. J. Chiang, G. N. Ali, G. T. C. Chiu, J. P. Allebach, and E. J. Delp, "Printer Identification Based on Textural Features", in *Proceedings of the IS&T's NIP20: International Conference on Digital Printing Technologies*, 2004, pp. 306-311.
- [7] A. K. Mikkilineni, G. N. Ali, P.J. Chiang, G. T. C. Chiu, J. P. Allebach, and E. J. Delp, "Signature-embedding in printed documents for security and forensic applications", in *Proceedings of the SPIE International Conference on Security, Steganography, and Watermarking of Multimedia Contents VI*, Jun 22 2004, pp. 455-466.
- [8] A. K. Mikkilineni, O. Arslan, P. J. Chiang, R. M. Kumontoy, J. P. Allebach, G. T.-C. Chiu and E. J. Delp, "Printer Forensic Using SVM Techniques", in *Proceedings of the IS&T's NIP21: International Conference on Digital Printing Technologies*, 2005, pp. 223-226.
- [9] A. K. Mikkilineni, P. J. Chiang, G. N. Ali, G. T. C. Chiu, E. J. Delp and J. P. Allebach, "Printer Identification Based on Graylevel Cooccurrence features for Security and Forensic Applications", in *Proceedings of the SPIE International Conference on Security, Steganography, and Watermarking of Multimedia Contents VII*, 2005, vol. 5681, p430-440.
- [10] O. Arslan, R. M. Kumontoy, P.J. Chiang, A.K. Mikkilineni, J. P. Allebach, G. T. C. Chiu and E. J. Delp, "Identification of Inkjet Printers for Forensic Applications", in *Proceedings of the IS&T's NIP21: International Conference on Digital Printing Technologies*, 2005, pp. 235-238.
- [11] A. K. Mikkilineni, P. J. Chiang, S. Suh, G. T. C. Chiu, J. P. Allebach and E. J. Delp, "Information embedding and extraction for electrophotographic printing processes", *Proceedings of the SPIE International Conference on Security, Steganography, and Watermarking of Multimedia Contents VIII*, 2006, vol. 6072, pp. 385-396.
- [12] P. J. Chiang, G. N. Ali, A. K. Mikkilineni, E. J. Delp, J. P. Allebach, and G. T.C. Chiu, "Extrinsic Signatures Embedding Using Exposure Modulation for Information Hiding and Secure Printing in Electrophotography", in *Proceedings of the IS&T's NIP20: International Conference on Digital Printing Technologies*, 2004, pp. 295-300.
- [13] P. J. Chiang, Mikkilineni, O. Arslan, R.M. Kumontoy, G. T.C. Chiu, E. J. Delp and J. P. Allebach, "Extrinsic Signatures Embedding in Text Document Using Exposure Modulation for Information Hiding and Secure Printing in Electrophotography", in *Proceedings of the IS&T's NIP21: International Conference on Digital Printing Technologies*, 2005, pp. 231-234.
- [14] P. J. Chiang, G. N. Ali, A. K. Mikkilineni, E. J. Delp, J. P. allebach and G. T. C. Chiu, "Extrinsic Signatures Embedding and Detection for Information Hiding and Secure Printing in Electrophotography" , in *Proceedings of the 2006 American Control Conference*, Jun 2006, pp. 2539-2544.
- [15] P. J. Chiang, Mikkilineni, E. J. Delp, J. P. Allebach and G. T.C. Chiu, "Extrinsic Signatures Embedding and Detection in Electrophotographic Halftone Images through Laser Intensity Modulation", in *Proceedings of the IS&T's NIP22: International Conference on Digital Printing Technologies*, 2006, pp. 432-435.
- [16] A. K. Mikkilineni, P. J. Chiang, E. J. Delp, J. P. Allebach and G. T.C. Chiu, "Data Hiding Capacity and Embedding Techniques for Printed Text Documents", in *Proceedings of the IS&T's NIP22: International Conference on Digital Printing Technologies*, 2006, pp. 432-435.
- [17] E. M. Williams, *The Physice adn Technology of Xerographic Processes*. New York: Wiley, 1984.
- [18] D. Kacker, T. Camis and J. P. Allebach, Electrophotographic Process Embedded in Direct Binary Search, *IEEE Trans. On Image Processing*, 11, p234-257, 2002
- [19] L. B. Schein, *Electrophotography and Development Physics*. Morgan Hill, CA: Laplacian Press, 1992.
- [20] P. G. J. Barten, "Evaluation of Subjective Image Quality with the Square-root Integral Method", *Journal of Optical Society of America A*, 7, 1990, no. 10, pp. 2024-2031.
- [21] F. W. Campbell and J. G. Robson, "Application of Fourier Analysis to the Visibility of Gratings", *J Physiol*. 1968 August; 197(3): 551-566G.